Fermi surface determination from wavevector quantization in LaSrCuO films

D. Ariosa,[a] C. Cancellieri,[b] P. H. Lin, and D. Pavuna
Laboratory of X-ray, IPMC-FSB-EPFL, Lausanne CH-1015, Switzerland

(Received 30 January 2008; accepted 14 February 2008; published online 6 March 2008)

We have observed the wavevector quantization in LaSrCuO films thinner than 12 unit cells grown on $SrTiO_3$ substrates. Low energy dispersions were determined *in situ* for different photon energies by angle resolved photoemission spectroscopy. From the wavevector quantization, we extract three dimensional dispersions within a tight-binding model and obtain the Fermi surface topology, without resorting to the nearly free-electron approximation. Such method can be extended to similar confined electron nanostructures. © *2008 American Institute of Physics*. [DOI: 10.1063/1.2891813]

Electron wavevector quantization (WVQ) in spatially confined solids has been observed for a variety of different systems including quantum wells (QWs) in thin films and nanostructures.[1–4] The effect is due to the discrete nature of the energy spectra associated with the standing wave solutions of the Schrödinger equation in a finite medium.[5] However, due to the roughness of their surfaces and interfaces, it is often not observed in very thin films. Namely, the observation of QW states requires interfaces that are smoother than the electron wavelength, which is of the order of a few atomic monolayers. In addition, it requires specific conditions in order to be directly observed by photoemission on thin cuprate films: (a) existence of the band dispersion along the confinement direction and (b) resolution in the electron wavevector better than the separation between the adjacent levels. As shown in the earlier publication,[6] condition (a) is fulfilled in the particular case of present work, as we have observed a pronounced three dimensional (3D) character in the electronic band dispersion of ultrathin LaSrCuO (LSCO) films with growth induced epitaxial in-plane tensile strain. Condition (b) is also fulfilled: the measurements were performed at the Synchrotron Radiation Center in Wisconsin on the 6 m planar grating monochromator (PGM) beamline by means of SCIENTA SES 2002 analyzer with an energy resolution of better than 10 meV and a momentum resolution of about 0.04 $Å^{-1}$. In this letter, we report a series of angle resolved photoemission spectroscopy (ARPES) measurements on ultrathin LSCO films performed at different photon energies exhibiting the WVQ. We also show how one can extract the 3D dispersions and the Fermi surface topology within a tight-binding scheme, without resorting to nearly free-electron approximation (NFEA). Such an approach is of interest and can be extended to other similar confined systems.

The photon energies are chosen in the range of 55–70 eV. The sample is placed in an ultrahigh vacuum chamber ($<10^{-10}$ mbar) and mounted on a coldfinger, which can be cooled down to 11 K. The analyzer is oriented for horizontal polarization. LSCO thin films are grown *in situ* on (100) $SrTiO_3$ single crystal substrates by pulsed laser deposition (PLD) as described in the previous work.[6–9] Their total thickness is accurately determined from the finite-size oscillations of the x-ray diffraction (XRD) peaks in a Bragg-Brentano geometry; notice that finite size oscillations in XRD require the same high interface quality as for WVQ to be observed. In Fig. 1(a), we show the momentum distribution curves (MDCs) observed for 12 unit cell (UC) sample, hole doped at $x=0.2$, at a photon energy of 62 eV, measured along $[\Gamma \rightarrow M]$, the nodal direction in the first Brillouin zone. In Fig. 1(b), we illustrate the band dispersion at another photon energy (67 eV), obtained from the maxima of the corresponding MDCs, on the same sample.

The observed staircase structure can be easily interpreted in terms of WVQ for 3D band dispersion: the probing surface[10] for the given photon energy intersects the set of quantized constant $k_z^{(n)}$ planes in the reciprocal space. At each intersection, for a given in-plane direction ($[\Gamma \rightarrow M]$ in Figs. 1 and 2), the photon is probing a particular electronic state of the $k_z^{(n)}$ branch. However, due to the finite momentum resolution, electrons in the considered branch can be photoemitted in a finite angular interval around the corresponding allowed k_z value, highlighting a finite segment of the discrete $k_z^{(n)}$ branch. The observed steps between consecutive branches are of about 20 meV, well above our estimated instrumental resolution.

Our measurements are reproducible and the discrete aspect of the dispersion is observed at different photon energies

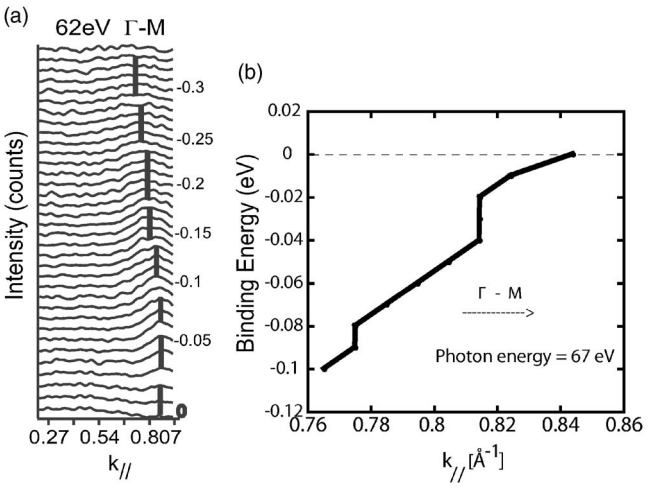

FIG. 1. (a) MDCs at a photon energy of 62 eV and (b) discrete band dispersion obtained at 67 eV along the nodal direction in a 12-UC $La_{1.8}Sr_{0.2}CuO_4$ (LSCO) thin film.

[a]Electronic mail: daniel.ariosa@epfl.ch.
[b]Electronic mail: claudia.cancellieri@epfl.ch.

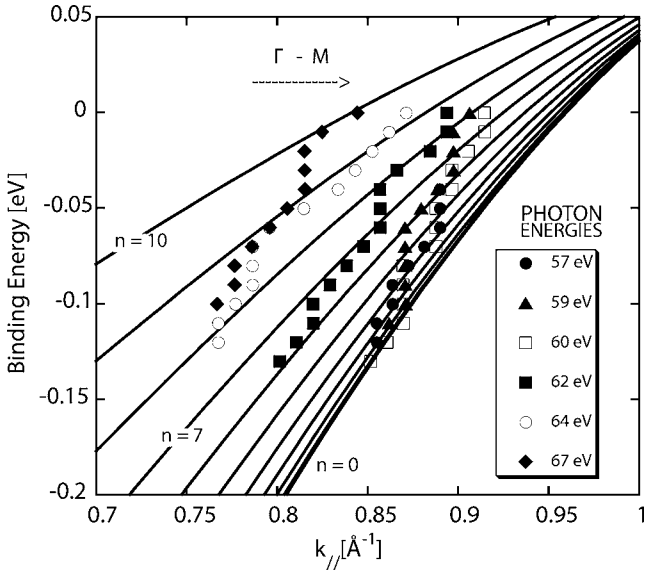

FIG. 2. Dispersion obtained at different photon energies and fits with the discrete 3DTB model for quantum levels indexed by $n=0,\ldots,10$.

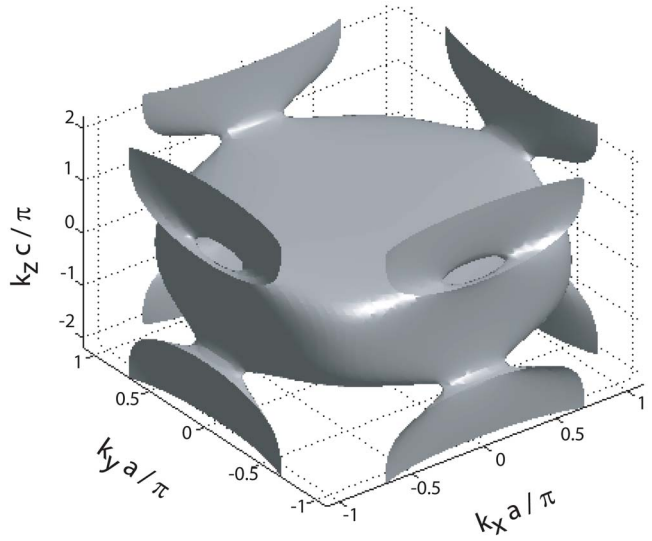

FIG. 3. (Color online) Reconstructed 3D Fermi surface using the band parameters from the fit in Fig. 2.

for all film thicknesses below 18 UC (230 Å). The expression for the quantized electron wavevector k_z for such z-axis confined system reads[5]

$$k_z^{(n)} = \frac{n\pi}{L} = \frac{n\pi}{Nc}, \tag{1}$$

where n is an integer and L is the confinement length, which in our case is simply Nc: the number of UCs times the crystal c-axis length. The critical thickness of 230 Å corresponds, thus, to a limit in wavevector resolution of 0.013 $Å^{-1}$, in good qualitative agreement with the nominal instrumental resolution.

In Fig. 2, we show the band dispersion obtained at six different photon energies for the same sample as in Fig. 1, together with the calculated discrete dispersion branches at constant $k_z^{(n)}$, obtained from the first 11 quantum levels $(n=0\ldots,10)$. To fit the dispersion, we use a discrete version of the generic 3D tight-binding (3DTB) model discussed in Ref. 6,

$$\begin{aligned} E_b^{(n)}(\mathbf{k}) = (\mu - E_F) - 2t[\cos(k_x a) + \cos(k_y a)] \\ + 4t' \cos(k_x a)\cos(k_y a) \\ - 8t'' \cos\left(\frac{k_x a}{2}\right)\cos\left(\frac{k_y a}{2}\right)\cos\left(\frac{n\pi}{2N}\right) \\ + 2t''' \cos\left(\frac{n\pi}{N}\right). \end{aligned} \tag{2}$$

From the fit in Fig. 2, we find the following band parameters: $t=17$ meV; $t'=4.42$ meV; $t''=149.6$ meV; $t'''=5.1$ meV. The Luttinger sum rule,[11] which applies to the 2D restriction of the band dispersion,[6] expanded linearly in $r=t'/t$ about half-filling yields: $(\mu-E_F)/t=2x+2.24r\simeq 0.98$. The number of UC is fixed at $N=12$, as extracted from finite size oscillations observed in XRD.

Due to the nonconservation of the normal component of the wavevector across the sample surface, the extraction of the 3D band parameters from ARPES data usually relies on the NFEA. The NFEA for the electron in the excited state contains two additional adjustable parameters: the photoelectron effective mass and the crystal inner potential.[12] In our case, the NFEA has difficulties to describe the observed dispersions since these two adjustable parameters, describing the probing surface in the reciprocal space, strongly depend upon the photon energy. Furthermore, within this approach, the band parameters also show significant variations with the photon energy. Conversely, the fit that uses our discrete approach is very consistent for all photon energies and probing directions in the momentum space. Within the discrete model, the number of adjustable parameters is reduced to 4; hence, the amount of data obtained by using several photon energies is highly redundant, conferring the fit of a high degree of reliability. Actually, by choosing the proper photon energy (e.g., 62 eV in our case), the experiment probes three consecutive levels and therefore, by adjusting four band parameters, one can easily fit the slope, the curvature, the quantum level separation, and the global scale in an almost unique way. Evidently, the above procedure requires the knowledge of the band filling (hole doping) and the exact number of UCs. Finally, by inserting the band parameters obtained from the fit in the continuous version of Eq. (2), one can reconstruct the 3D Fermi surface, as illustrated in Fig. 3. The obtained FS is the continuous envelope of the discrete one.

The failure of the usual NFEA in trying to fit experimental single photon energy data within the 3DTB approach is due to the impossibility to retrieve the experimental probing path in the reciprocal space. Namely, by adjusting the photoelectron effective mass and the inner potential, the projected path in the $E_b(k_\parallel)$ graph should intersect the consecutive segments of the band dispersion close to their center. In practice, this path has a limiting slope which prevents such an intersection for reasonable values of the band parameters. On the other hand, the periodic potential seen by the photoelectron is highly anisotropic in high temperature superconductors (HTSC) oxides. Therefore, the effective mass in the NFEA should reflect the anisotropy of the layered material. The expression for the normal component k_z with the effective mass anisotropy becomes

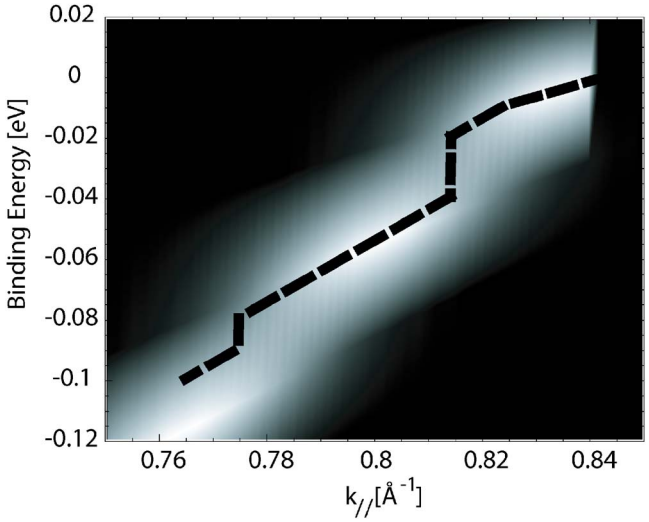

FIG. 4. (Color online) Simulation of ARPES experiment. The dashed line represents experimental data.

$$k_z = \sqrt{\frac{2m^*}{\hbar^2}(E_{\rm ph} + |E_0| + E_b) - \lambda k_\parallel^2} - G_z. \tag{3}$$

By including an anisotropy factor $\lambda = m_c^*/m_{ab}^* = 3.25$ for the 67 eV data, with an inner potential (excluding the work function) $|E_0| = 8.55$ eV, we find the correct projection of the probing path. The reciprocal lattice vector G_z is defined in the footnote.[10] In order to illustrate our analysis, a numerical simulation of the photoemission intensity (see Fig. 4) is carried out within the anisotropic NFEA using the tight-binding parameters found with the discrete fit. We include the effective resolution by assuming a fixed Gaussian spread $\Sigma = 0.01$ Å^{-1} for the k_z vector,

$$I(k_\parallel, E_b) = I_0 \frac{1}{\sqrt{2\pi\Sigma^2}} \sum_n \exp\left(-\frac{(k_z - k_z^{(n)})^2}{2\Sigma^2}\right). \tag{4}$$

Equation (4) simply collects the intensity contributions from the discrete dispersion branches at each given point $(k_\parallel, E_b)$. The different quantized branches are probed by the broad distributed wavevector centered at the k_z value given by Eq. (3), the anisotropic NFEA. Consequently, the actual resolution of our experiment is a combination of the intrinsic instrumental resolution and the strength of the 3D dispersion that determines the separation between consecutive energy levels.

Therefore, by including an effective mass anisotropy in the NFEA, the probing surface in momentum space for single photon energy ARPES experiments is correctly described accounting for the observed staircase structure due to the combined effect of the WVQ and finite instrumental resolution. Present analysis constitutes the methodological basis for our systematic, on-going investigations of the strain and size effects on the electronic structure of ultrathin HTSC LSCO films discussed elsewhere.

In summary, we have observed the wavevector quantization in ultrathin HTSC LaSrCuO films (thinner than 12 UCs) grown on $SrTiO_3$ substrates by laser ablation. Low energy dispersions were determined at different photon energies by ARPES. The strength of our simple approach is the extraction of the 3D band dispersion and the resulting Fermi surface without resorting to the NFEA. Instead, we take advantage of the WVQ along the surface normal and fit dispersion curves within the tight-binding model. Such simple method can be applied to other similar confined electron systems of interest in nanoscience and nanotechnology.

We thank the Dean of Basic Sciences of EPFL for a special financial support and Hartmut Höchst for his valuable scientific support during the beamtime at SRC (Madison). We are also grateful to David Oezer (EPFL) for his assistance on film structural characterization. This work was supported by the Swiss National Science Foundation, the EPFL, and the National Science Council of Taiwan under Grant No. NSC 95-2475-M-01-010. The experiments were performed at the UW-SRC, supported by NSF under Grant No. DMR-0537588.

[1] I. Matsuda, T. Tanikawa, S. Hasegawa, H. W. Yeom, K. Tono, and T. Ohta, e-J. Surf. Sci. Nanotechnol. **2**, 169 (2004).
[2] P. Segovia, E. G. Michel, and J. E. Ortega, J. Vac. Sci. Technol. A **16**, 1368 (1998).
[3] K. Pedersen, P. Morgen, T. Garm Pedersen, Z. Li, and S. V. Hoffmann, J. Vac. Sci. Technol. A **21**, 1431 (2003).
[4] G. Rodary, D. Sander, H. Liu, H. Zhao, L. Niebergall, V. S. Stepanyuk, P. Bruno, and J. Kirschner, Phys. Rev. B **75**, 233412 (2007).
[5] T. Balcerzak, Thin Solid Films **500**, 341 (2006).
[6] D. Cloetta, D. Ariosa, C. Cancellieri, M. Abrecht, S. Mitrovic, and D. Pavuna, Phys. Rev. B **74**, 014519 (2006).
[7] D. Ariosa, M. Abrecht, D. Pavuna, and M. Onellion, Proc. SPIE **4058**, 129 (2000).
[8] M. Abrecht, T. Schmauder, D. Ariosa, O. Touzelet, S. Rast, M. Onellion, and D. Pavuna, Surf. Rev. Lett. **7**, 495 (2000).
[9] M. Abrecht, D. Ariosa, D. Cloetta, S. Mitrovic, M. Onellion, X. X. Xi, G. Maragaritondo, and D. Pavuna, Phys. Rev. Lett. **91**, 057002 (2003).
[10] The probing surface for a given photon energy is located between two concentric spheres centered at $(0,0,-G_\perp)$ with slightly different radii $\sqrt{(2m^*[E_{\rm ph}+|E_0|+E_b(0)])/\hbar^2}$, for the maximal binding energy (Γ point) and, $\sqrt{[2m^*(E_{\rm ph}+|E_0|)]/\hbar^2}$, for zero binding energy (Fermi level). The reciprocal lattice vector $G_\perp$ is defined as $G_\perp \approx \sqrt{[2m^*(E_{\rm ph}+|E_0|)]/\hbar^2}$, $E_{\rm ph}$, $|E_0|$, and E_b are the photon energy, the inner potential, and the binding energy, respectively.
[11] J. M. Luttinger, Phys. Rev. **119**, 1153 (1960).
[12] S. Hüfner, *Photoelectron Spectroscopy: Principles and Applications* (Springer, Berlin, 2003).